

Intra-annual Principal Modes and Evolution Mechanism of the El Niño/Southern Oscillation

Yongwen Zhang,^{1,2} Jingfang Fan,³ Xiaoteng Li,⁴ Wenqi Liu,¹ and Xiaosong Chen^{5, a)}

¹⁾*Data Science Research Center, Faculty of Science, Kunming University of Science and Technology, Kunming 650500, China;*

²⁾*Department of Physics, Bar-Ilan University, Ramat Gan 52900, Israel;*

³⁾*Potsdam Institute for Climate Impact Research, 14412 Potsdam, Germany;*

⁴⁾*Harvest Found Management Co., Ltd, 100005 Beijing, China;*

⁵⁾*School of Systems Science, Beijing Normal University, Beijing 100875, China*

(Dated: 31 March 2020)

The El Niño-Southern Oscillation (ENSO) is one of the most important phenomena in climate. By studying the fluctuations of surface air temperature within one year between 1979-01-01 and 2016-12-31 of the region (30°S-30°N, 0°E-360°E) with eigen-decomposition, we find that the temperature fluctuations are dominated by the two principal modes whose temporal evolutions respond significantly to the ENSO variability. According to introduce a “micro-correlation”, we find that the coupling between the first principal mode and the temperature fluctuations in the El Niño region could result in different ENSO phases. Without this coupling, the El Niño region is in a normal phase. With the strong coupling between the El Niño region and the Northern Hemisphere, an El Niño event will appear with a high probability. Then this coupling changes to be strong between the El Niño region and the Southern Hemisphere accounting for the fast decay of El Niño after boreal winter, even leading to a La Niña event. Moreover, the coupling between the El Niño region and the second principal mode is found to be strong in normal or La Niña phases in response to the normal or strong Walker Circulations. We conjecture that the temporal evolutions of these couplings for the first and second principal modes are controlled by the meridional and zonal ocean-atmospheric circulations respectively.

PACS numbers: Valid PACS appear here

Keywords: Suggested keywords

I. INTRODUCTION

The complexities of climate systems are generally due to the existence of multi-scales phenomena¹, which have a wide variety of space and time scales. Small-scale phenomena such as convection and precipitation² assumed to be driven by large-scale forces such as extratropical cyclones, planetary-scale waves, and meridional circulations that extend over thousands of kilometers to transport energy between the tropics and the polar regions. The El Niño/Southern Oscillation (ENSO), referring to vary between anomalously warm (El Niño) and cold (La Niña) phases in eastern Pacific, can cause the global impacts on year-to-year time scales^{3,4}. In 1969, Bjerknes postulated that the Bjerknes feedback (the Walker circulation) was essential to the ENSO⁵. Still, the mechanism of ENSO has not been fully understood⁶. The alternation between warm and cold phases is quite irregular⁷. There was controversy over whether the ENSO is controlled by stochastic processes⁸. Teleconnections

^{a)}Electronic mail: chenxs@bnu.edu.cn

are widely observed near the equator, since heat frequently exchanges between the ocean and atmosphere in the region, and energy is transported over a great distance from the region by the general circulations^{9,10}. From the physics point of view, a small-scale fluctuation could trigger abrupt changes in large-scale, if the precondition is satisfied that the system exits long-range correlations (teleconnections).¹¹⁻¹³. Thus the ENSO could be triggered by small-scale and short-term processes.

Although the ENSO is as well known as an inter-annual phenomenon, a significant intra-annual property of the ENSO has been found that it is the synchronization with annual cycle—El Niño events tend to peak in boreal winter and fall rapidly in boreal spring^{14,15}. To capture this synchronization and the rapid termination of El Niño events, the interaction between inter-annual and intra-annual timescales need to be considered¹⁶⁻¹⁸. The ENSO could be coupling with intra-annual oscillations¹⁹⁻²², even with higher frequency processes^{23,24}.

Eigen analysis has been a classic technique to distinguish multiple physical processes into a combination of some single processes and capture the individual feature. It is widely used in community detection, image recognition and empirical data analysis²⁵⁻²⁷. It has also emerged as a popular tool in climate science²⁸ and been used to search for the important features of the ENSO²⁹⁻³¹. Inter-annual principal modes associated with the ENSO are found based on eigen analysis^{16,29}. On the other hand, other methods such as climate networks have also been used to study and predict the El Niño in recent decades³²⁻³⁹. Actually, the essential of climate networks depends on the correlation matrix as well as the eigen method^{40,41}.

Here, we use eigen analysis to study the principal modes of daily surface air temperature. Note that we use the original temperature rather than abnormal temperature. Previous studies²⁹⁻³¹ mentioned above focused mainly on the inter-annual principal modes after removal of seasonality. Instead, we investigate the intra-annual principal modes including seasonality. According to eigen-decomposition for a correlation matrix in a 365 days' window, the principal modes will be obtained. The dynamics of the principal modes will be detected by the temporal evolution of the eigenvalues and eigenvectors. The properties of eigenvalues usually were neglected by the previous studies. From a physical perspective, eigenvalues play an important role to describe macroscopic properties in a physical system^{42,43}. Furthermore, the detailed spatial patterns are performed by the distributions of eigenvectors. This paper is organized as follows. Section II describes the methods and data. In section III we presented the results, and provides the conclusions in section IV.

II. DATA AND METHODOLOGY

A. Data

Our study is based on daily surface air temperature (2 m) and wind (10 m) provided by the European Centre for Medium-Range Weather Forecasts Interim Reanalysis (ERA-Interim)⁴⁴ on a $2.5^\circ \times 2.5^\circ$ latitude-longitude grid over the region (30°S - 30°N , 0°E - 360°E), resulting in $25 \times 144 = 3600$ grids. The dataset spans the time period between 1979-01-01 and 2016-12-31. El Niño or La Niña events are defined when the Oceanic Niño Index (ONI) exceed $\pm 0.5^\circ\text{C}$ for a period of five months or more. The ONI is defined as 3 month running mean of ERSST.v5 SST anomalies in the El Niño 3.4 region (5°S - 5°N , 190°E - 240°E).

B. Methodology

In a climate system consisting of N grids, the temperature of a grid i at time t within a time window of length d is defined as $S_i(t; T)$, where T represents the central time of the

time window. The average temperature of grid i for the time window is calculated as

$$\bar{S}_i^T = \frac{1}{d} \sum_{t=1}^d S_i(t; T). \quad (1)$$

At the time t , the grid i has a temperature fluctuation $\delta S_i(t; T) = S_i(t; T) - \bar{S}_i^T$. The normalized fluctuation $\delta \hat{S}_i(t; T) = \delta S_i(t; T) / \sqrt{\langle [\delta S_i(t; T)]^2 \rangle}$. The correlation of temperature for the time window between grids i and j is defined as

$$C_{ij}(T) = \langle \delta \hat{S}_i(t; T) \cdot \delta \hat{S}_j(t; T) \rangle, \quad (2)$$

which is the Pearson correlation coefficient. Using $C_{ij}(T)$ as its elements, we obtain then a $N \times N$ correlation matrix $\mathbf{C}(T)$ with N eigenvectors and eigenvalues. The eigenvector corresponding to eigenvalue $\lambda_n(T)$ is $\mathbf{b}_n(T)$ which satisfies the equation

$$\mathbf{C}(T) \cdot \mathbf{b}_n(T) = \lambda_n(T) \mathbf{b}_n(T), \quad n = 1, 2, \dots, N. \quad (3)$$

The eigenvalues are numbered in the order $\lambda_1(T) \geq \lambda_2(T) \cdots \geq \lambda_N(T) \geq 0$. The eigenvectors follow the condition

$$\mathbf{b}_n(T) \cdot \mathbf{b}_l(T) = \sum_i b_{in}(T) b_{il}(T) = \delta_{nl}, \quad (4)$$

where $\delta_{nl} = 1$ at $n = l$ and $\delta_{nl} = 0$ otherwise. All eigenvectors are normalized and orthogonal to each other.

Using the n -th eigenvector $\mathbf{b}_n(T)$, the n -th principal mode can be obtained as

$$a_n(t; T) = \sum_{i=1}^N b_{in}(T) \delta \hat{S}_i(t; T). \quad (5)$$

The correlation between principal modes $\mathbf{a}_n(T)$ and $\mathbf{a}_l(T)$ is

$$\langle \mathbf{a}_n(T) \cdot \mathbf{a}_l(T) \rangle = \frac{1}{d} \sum_{t=1}^d a_n(t; T) a_l(t; T) = \lambda_n(T) \delta_{nl}. \quad (6)$$

So different principal modes are independent. The square amplitude of a principal mode is equal to the corresponding eigenvalue.

$\delta \hat{S}_i(t; T)$ can be considered also as the summation of contributions from all principal modes

$$\delta \hat{S}_i(t; T) = \sum_{n=1}^N b_{in}(T) a_n(t; T). \quad (7)$$

Combining Eq. 7 and Eq. 6 into Eq. 2, the correlation between grids i and j can be written as

$$C_{ij}(T) = \sum_{n=1}^N b_{in}(T) b_{jn}(T) \lambda_n(T). \quad (8)$$

To quantify the averaged correlation between a region A and a region B for the positive components of the n -th eigenvector, a "micro-correlation" is introduced as

$$C_{AB}^{n+}(T) = \frac{\sum_{i \in A} \sum_{j \in B} \Theta_{in}^+ b_{in}(T) \Theta_{jn}^+ b_{jn}(T) \lambda_n(T)}{\sum_{i \in A} \sum_{j \in B}}, \quad (9)$$

where $\Theta_{in}^+ = 1$, when $b_{in}(T) > \Delta$, otherwise $\Theta_{in}^+ = 0$. Δ is a positive threshold to exclude weak and negative components. The definition of "micro-correlation" for the negative components $C_{AB}^{m-}(T)$ is similar, only $\Theta_{in}^+, \Theta_{jn}^+$ change to $\Theta_{in}^-, \Theta_{jn}^-$, where $\Theta_{in}^- = 1$, when $b_{in}(T) < -\Delta$, otherwise $\Theta_{in}^- = 0$.

Furthermore, we can shift the time T to get a series of correlation matrices $\mathbf{C}(T)$. Then the evolution of principal modes will be obtained. Note that different principal modes for different T are not independent.

III. RESULTS

Since the seasonal cycle is 365 days, we take the length of time window $d = 365$. For a time window with its center in the month T , we can obtain the correlation matrix $\mathbf{C}(T)$, its eigenvalues $\lambda_n(T)$, and the corresponding eigenvectors $\mathbf{b}_n(T)$. With T shifted by one month each time, their evolution with time can be obtained. The first eigenvalues $\lambda_1(T)$ and the second eigenvalues $\lambda_2(T)$ with T from 1979.06 to 2016.06 are shown in Fig. 1(a) and (b). The ratio of the first eigenvalue $\lambda_1(T)/\sum_n \lambda_n(T)$ is more than 40%. The second eigenvalue has the ratio $\lambda_2(T)/\sum_n \lambda_n(T)$, which is more than 10%. So the temperature fluctuations in the region are dominated by these two principal modes.

We study at first the evolution of eigenvalues. After comparing $\lambda_1(T)$ with the ONI, we find a strong positive relevance between them. The peaks of $\lambda_1(T)$ correspond to the El Niño events and its valleys correspond to the La Niña events (see Fig. 1(a)). The overall correlation between $\lambda_1(T)$ and the ONI is characterized by their Pearson correlation coefficient, which is equal to 0.65. The Pearson correlation coefficient between $\lambda_2(T)$ and the ONI is equal to -0.62 . So λ_2 is negatively correlated to the ONI (see Fig. 1(b)). Moreover, the Pearson correlation coefficient between λ_1 and λ_2 is calculated and equal to -0.75 . This indicates that the temporal evolution of $\lambda_1(T)$ is opposite to $\lambda_2(T)$.

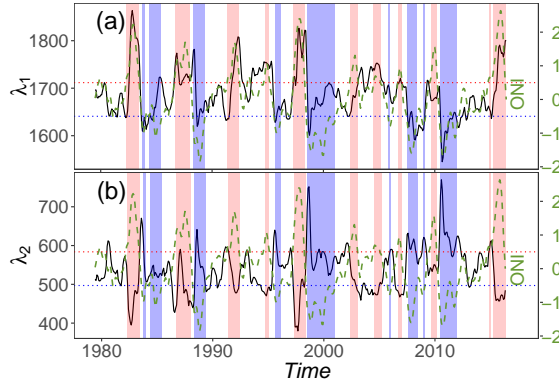


FIG. 1. The first eigenvalue λ_1 (a) and the second eigenvalue λ_2 (b) as functions of time T (black solid line, left scale). The green dash line is the Oceanic Niño Index (ONI) (right scale). Red and blue shades represent respectively El Niño and La Niña periods.

From temperature fluctuations $\delta\hat{S}_i(t;T)$ and eigenvector $\mathbf{b}_n(T)$, we can get the intra-annual principal mode $\mathbf{a}_n(T)$ by Eq. 5. The principal mode $\mathbf{a}_n(T)$ is related to the eigenvalue by Eq. 6. In Fig. 2, the principal modes $a_1(t;T)$ and $a_2(t;T)$ are shown with respect t at different T corresponding to a normal time (1994.01), an El Niño time (1998.01), and a La Niña time (2000.01) respectively. A dominant seasonal oscillation in the first principal mode $a_1(t;T)$ is observed and presented in Fig. 2(a). The maximum and minimum of $a_1(t;T)$ are located in mid February and mid August, which correspond respectively to winter and summer in the Northern Hemisphere. In the first principal mode $a_1(t;T)$, there are positive temperature fluctuations between mid November to next mid May and negative temperature fluctuations from mid May to mid November.

The second principal mode $a_2(t; T)$ is presented in Fig. 2(b), where a seasonal oscillation is also observed. In comparison with $a_1(t; T)$, the seasonal oscillation of $a_2(t; T)$ has a shift. In relation to $a_2(t; T)$, there are positive temperature fluctuations from March to August and negative temperature fluctuations from August and next March.

The oscillation amplitude of $a_2(t; T)$ is smaller than that of $a_1(t; T)$. It is reasonable that the seasonal cycle plays the dominant role in $a_1(t; T)$ and $a_2(t; T)$, since the influences of Sun are the deciding factors to result in the fluctuations of surface air temperature. Besides the seasonal trend, there are only small differences of $a_1(t; T)$ and $a_2(t; T)$ for different T . Yet, these small differences can result in the significant correlations of $\lambda_1(T)$ and $\lambda_2(T)$ with the ONI.

We can express $\delta\hat{S}_i(t; T)$ by principal modes as Eq. 7. After taking into account the two dominant principal modes, we have

$$\delta\hat{S}_i(t; T) \approx b_{i1}(T)a_1(t; T) + b_{i2}(T)a_2(t; T). \quad (10)$$

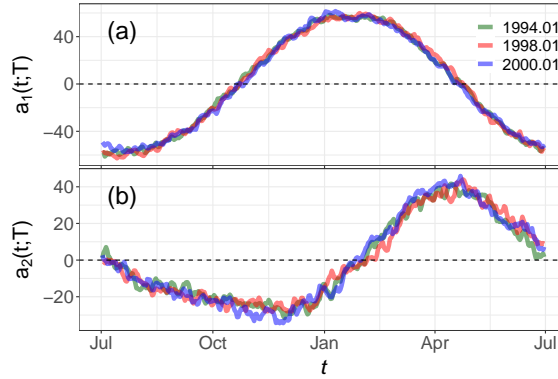


FIG. 2. (Color online) The (a) first and (b) second principal modes for the different T : 1994.01, 1998.01 and 2000.01.

To understand further the physical features of intra-annual principle modes, we need to study the spatial distribution of $\mathbf{b}_n(T)$. The components b_{i1} of the first eigenvector $\mathbf{b}_1(T)$ is depicted in Fig. 3 for T from 1997.01 to 1999.01, which spans the strong 97-98 El Niño event. The distributions of b_{i1} are divided mainly into two large clusters. One is in the Northern Hemisphere and has negative components. Another one is in the Southern Hemispheres and has positive components. In addition, there are two small clusters with negative components and located in the rainforests of Congo (Africa) and Amazon (South America). The components of the interface between two large clusters are nearly zero. The interface exists around the Equator and varies greatly with time T .

In the running 3-month DJF of 1997, the ONI was -0.49 and increased to 0.74 in the AMJ of 1997, which demonstrated the emergence of an El Niño event. This event lasted until to the MAM of 1998. With the further decrease of the ONI, a La Niña event appeared in the JJA of 1998 and lasted until 2001.

In the normal phase at the beginning, the El Niño 3.4 region (5°S - 5°N , 190°E - 240°E) belongs to the interface and the corresponding $b_{i1}(T)$ are nearly zero (see Fig. 3 for 1997.01). The temperature fluctuations in the region are nearly independent of the first principal mode. Later, the components $b_{i1}(T)$ in a part of the region become negative. The temperature fluctuations there are dominated by the first principal mode $\delta\hat{S}_i(t; T) \sim b_{i1}(T)a_1(t; T)$. The negative components (blue) in the El Niño 3.4 region (see Fig. 3 for 1997.04 and 1997.07) result in the temperature fluctuations increases as $a_1(t; T)$ decreases from February to August (see Fig. 2(a)) in comparison with the normal phase. Then an El Niño appeared, and the components in the El Niño region gradually change from negative to positive. We can see that the components $b_{i1}(T)$ in a part of the El Niño region become positive later (see Fig. 3 for 1998.04 and 1998.07). These positive components (red) can contribute the increase of temperature fluctuations when $a_1(t; T)$ increases from August to

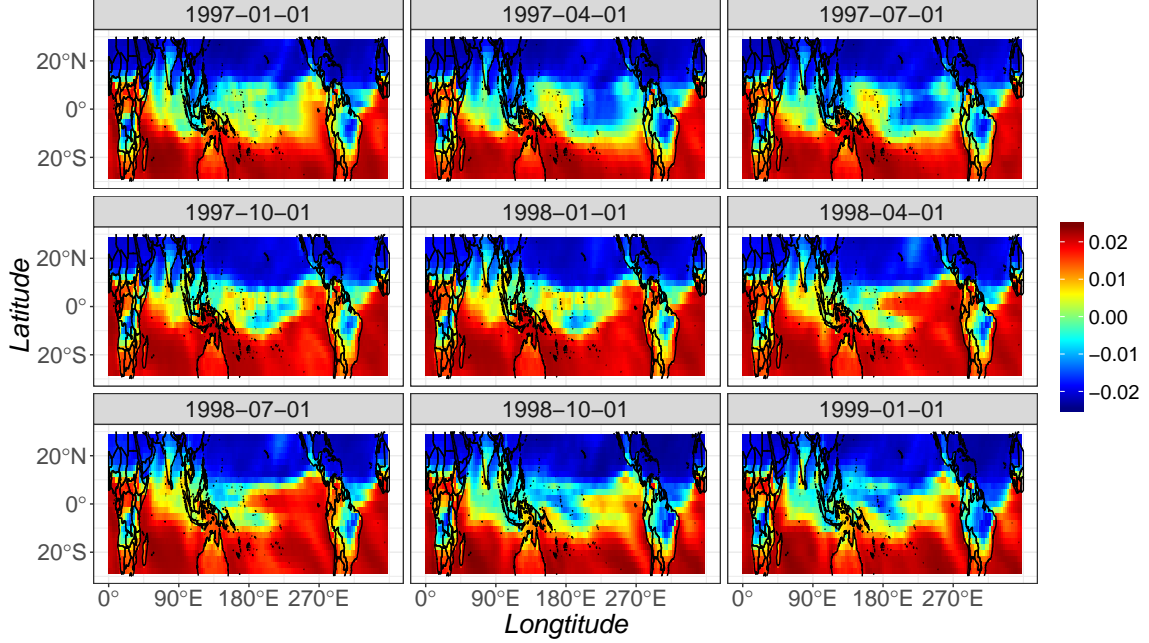


FIG. 3. (Color online) Spatial distributions of components of the first eigenvector $\mathbf{b}_1(T)$, where the time T is from 1997.01 to 1999.01. They are the normal (1997.01–1997.04), El Niño (1997.05–1998.05), and La Niña (1998.07–1999.01).

the next February. After February, $a_1(t; T)$ decreases very fast so that the positive components $b_{i1}(T)$ in the region lead to a strong decrease of temperature and end the El Niño, which lasts until August. There is a La Niña now.

The spatial distributions of $\mathbf{b}_2(T)$ are shown in Fig. 4. In the second principal mode, there are mainly two clusters with positive components and their temperature fluctuations are coupled. At the beginning of 1997, there is a large cluster with positive components in the Equatorial Eastern Pacific. With the emergence of El Niño from 1997.07 to 1998.04, this cluster becomes smaller and weaker. Even a cluster with negative components appears in the region. After the end of El Niño, there is a La Niña and a cluster with positive components appears again in the Eastern Pacific.

To further quantify the relationship between the ENSO and the spatial distributions of \mathbf{b}_n , we calculate the micro-correlation via Eq. 9. We take the threshold Δ as $\frac{1}{2\sqrt{N}} = 0.008$. The micro-correlation between the El Niño 3.4 region and the north region (5°N - 90°N , 0°E - 360°E) for the negative components of the first eigenvector can be obtained as C_{EN}^{1-} . Similarly we obtain the micro-correlation C_{ES}^{1+} between the El Niño 3.4 region and the south region (5°S - 90°S , 0°E - 360°E) for the positive components of \mathbf{b}_1 . The micro-correlation C_{EN}^{1-} (dashed line) and C_{ES}^{1+} (solid line) are shown as functions of time T in Fig. 5(a). A large C_{EN}^{1-} represents that the El Niño region is positively correlated with the Northern Hemisphere, as shown in Fig. 3. A large C_{ES}^{1+} represents that the El Niño region is positively correlated with the Southern Hemisphere. In normal phases, it can be seen in Fig. 5(a) that both C_{EN}^{1-} and C_{ES}^{1+} are weak. Indeed, we observed that C_{EN}^{1-} usually has a peak before the emergence of an El Niño event in Fig. 5(a). Instead, C_{ES}^{1+} has a sharp peak at the end of an El Niño event.

Thus the evolution of the micro-correlation C_{EN}^{1-} and C_{ES}^{1+} could demonstrate that the ENSO phenomenon is related to the competition of the influences from the Northern and Southern Hemispheres. When the influences from both Hemispheres are in balance, the El Niño region belongs to the interface of $\mathbf{b}_1(T)$ so that its temperature fluctuations are independent of the Northern and Southern Hemispheres. There is a normal phase in the region. When the influences from the Northern Hemisphere dominate, the upper part of El

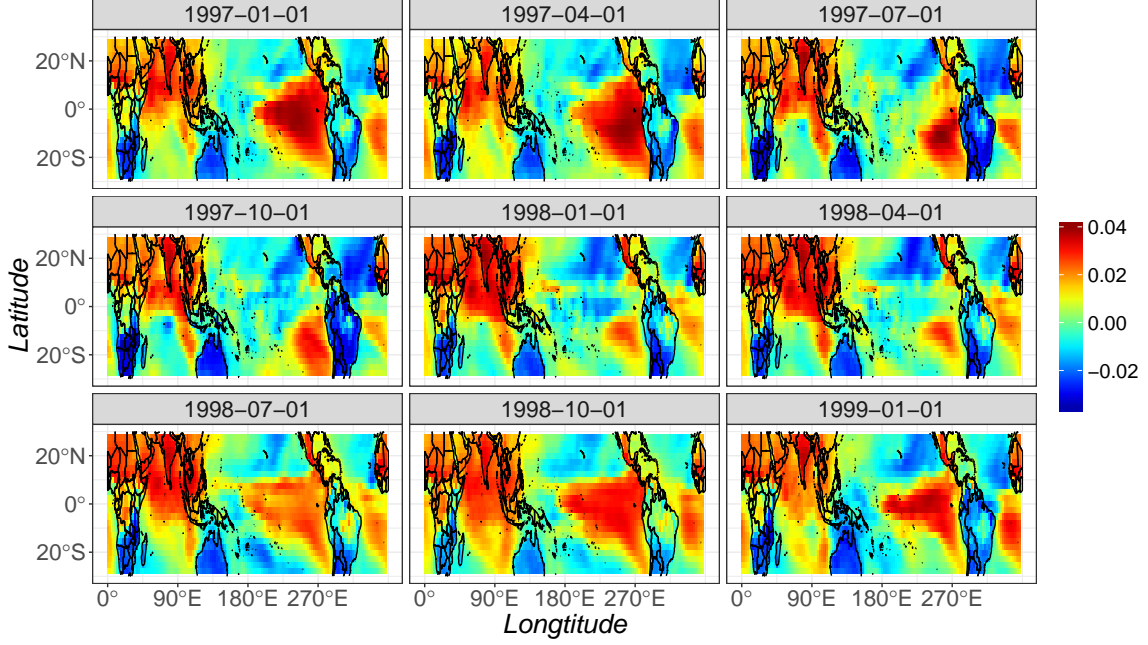


FIG. 4. (Color online) Same as Fig. 3 but for the second eigenvector $\mathbf{b}_2(T)$.

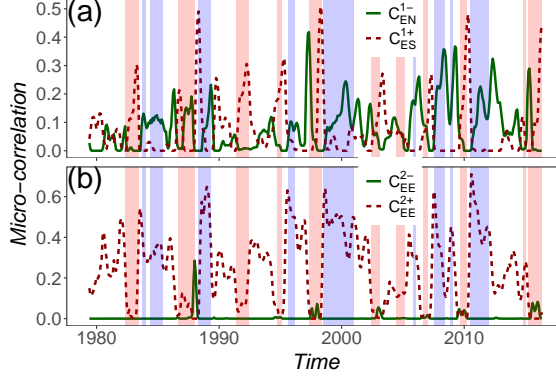


FIG. 5. (Color online) Micro-correlation for (a) the first eigenvector \mathbf{b}_1 and (b) the second eigenvector \mathbf{b}_2 . Red and blue shades represent respectively El Niño and La Niña periods.

Niño region is integrated into the northern cluster. The temperature increases in the El Niño region from February to August. Then, an El Niño event appears. If the influences from the Southern Hemisphere become dominant, the lower part of Niño region is integrated into the southern cluster. The temperature increases in the El Niño region until the next February, then fast decreases with the temperature of the Southern Hemisphere after February. We anticipate that the competition between the Northern and Southern Hemispheres in the first principal mode could be driven by the Hadley Circulation⁴⁵, which is a general meridional ocean-atmospheric circulation.

Since the second eigenvector \mathbf{b}_2 is dominated by the cluster with positive components in the Equatorial Eastern Pacific (see Fig. 4), we calculate the micro-correlation for the El Niño 3.4 region itself like auto-correlation. Then we get C_{EE}^{2-} and C_{EE}^{2+} for the negative and positive components respectively. Fig. 5(b) shows that C_{EE}^{2-} is always zero apart from during several El Niño events. The micro-correlation C_{EE}^{2+} is strong during La Niña phases and weak during El Niño phases in Fig. 5(b). It indicates that the strength of the cluster

in the El Niño region is anti-correlated with the ONI in this region. It seems to be related to the Walker Circulation, which is a zonal ocean-atmosphere circulation in the Pacific⁴. The east-west surface temperature contrast reinforces an east-west air pressure difference across the Pacific basin, which in turn drives trade winds. During La Niña, the Walker Circulation becomes stronger. During El Niño instead, the trade winds become weak as atmospheric pressure rises in the western Pacific and falls in the eastern Pacific. Then the Bjerknes feedback operates in reverse, with weakened trade winds and SST warming tendencies along the equator². The Walker Circulation can provide the force to reshape the largest cluster in the Eastern Pacific of \mathbf{b}_2 .

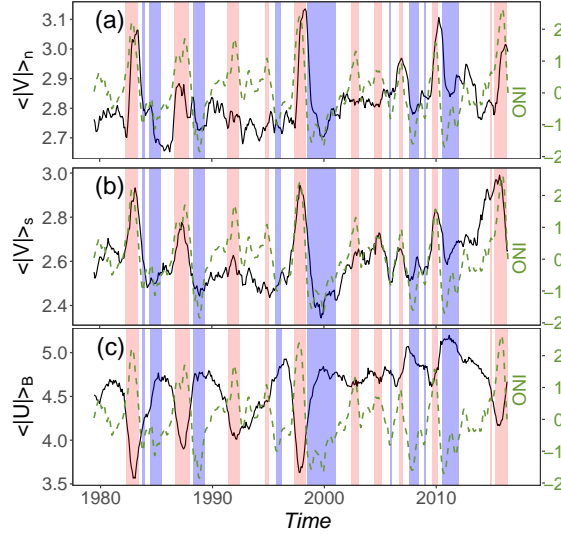


FIG. 6. The mean V wind strength (a) $\langle |V| \rangle_s$ and (b) $\langle |V| \rangle_n$, and (c) the mean U wind strength $\langle |U| \rangle_B$ as a function of time T .

We further prove our conjectures by studying the daily surface wind field (10 m). The wind is divided into meridional part V and zonal part U . For the northern region (0° - 30° N, 190° E- 270° E), the average magnitude $\langle |V| \rangle_n(T)$ is calculated and presented in Fig. 6(a). We make the average for one year with its center in the month T . The average magnitude of V in the southern region (0° - 30° S, 190° E- 270° E) is denoted as $\langle |V| \rangle_s(T)$. The results obtained are shown in Fig. 6(b). We can see that El Niño events are accompanied usually by strong $\langle |V| \rangle_{n,s}(T)$. In general, $\langle |V| \rangle_n(T)$ is larger than $\langle |V| \rangle_s(T)$. This result further demonstrates that the connection between the Equator and Northern (Southern) Hemisphere becomes stronger during El Niño in agreement with the results of the micro-correlation C_{EN}^{1-} and C_{ES}^{1+} in Fig. 5(a).

For the zonal part of wind, we calculate its average magnitude $\langle |U| \rangle_B(T)$ in the Niño 3 and 3.4 regions (5° S- 5° N, 190° E- 270° E). The results obtained are depicted in Fig. 6(c). During El Niño events, there are obvious decreases of $\langle |U| \rangle_B(T)$ as similar as C_{EE}^{2+} in Fig. 5(b).

IV. CONCLUSIONS

Here we study the principal modes of surface air temperature in the region (30° S- 30° N, 0° E- 360° E) within one year in relation to the El Niño/Southern Oscillation. They are dominated by the two largest intra-annual principal modes, which are obtained by the eigen-decomposition method. The temporal evolution of the principal modes is investigated from 1979-01-01 to 2016-12-31. Their eigenvalues λ_1 and λ_2 response oppositely to the ENSO variability. The Pearson correlation coefficients between the two eigenvalues and the ONI are equal to 0.65 and -0.62 , respectively.

Both principal modes exhibit significant seasonal oscillations. We propose an evolutionary mechanism of El Niño/Southern Oscillation based on the temporal evolution of the spatial distribution of two principal modes. The first principal mode $a_n(t; T)$ decreases as t from February to August, and increases from August to the next February. In normal phases, the El Niño region has weak coupling with the first principal mode and its temperature fluctuations are dominated by the second principal mode. When the coupling becomes strong between the El Niño region and the Northern Hemisphere between February and August, an El Niño event will occur with a high probability. As the evolution of the first eigenvector, the coupling changes to be strong between the El Niño region and the Southern Hemisphere. It causes that the temperature increases in the El Niño region, then fast decreases after the next February. We introduce the micro-correlation to quantify the correlations between the El Niño region and the Northern (Southern) Hemisphere for the principal mode. On the other hand, the coupling between the El Niño region and the second principal mode is strong in normal or La Niña phases in response to the normal or strong Walker Circulations. With the emergence of an El Niño event, this coupling becomes much smaller so that there is a much weaker Walker Circulation.

We suggest that the first and second intra-annual principal modes are related to the meridional and zonal circulations respectively. This is partly demonstrated by the mean meridional and zonal surface wind field (10 m). During El Niño events, there are stronger mean meridional wind and weaker mean zonal wind. The meridional circulations can drive the competition between the influences from the Northern and Southern Hemispheres that could determine the El Niño region to be in a normal, El Niño, and La Niña phases.

ACKNOWLEDGMENTS

We thank the financial support by the National Natural Science Foundation of China (Grant Nos. 61573173) and Key Research Program of Frontier Sciences, CAS (Grant No. QYZD-SSW-SYS019). We also acknowledge the computational resources provided by HPC Cluster of ITP-CAS. Data in support of this work can be found through the ERA-Interim reanalysis of the European Center for Medium-Range Weather Forecasts (<https://doi.org/10.1002/qj.828>).

¹D. Hartmann, *Global physical climatology* (Academic Press, 1994) pp. 159–162.

²J. D. Neelin, *Climate change and climate modeling* (Cambridge University Press, 2011) pp. 198–199.

³M. J. McPhaden, S. E. Zebiak, and M. H. Glantz, “ENSO as an integrating concept in earth science,” *Science* (80-.). **314**, 1740 (2006).

⁴C. Wang, C. Deser, J. Y. Yu, P. Dinezio, and A. Clement, *El Niño and Southern Oscillation (ENSO): A review* (Springer Netherlands, 2017).

⁵J. Bjerknes, “Atmospheric teleconnections from the Equatorial Pacific1,” *Mon. Weather Rev.* **97** (1969).

⁶M. J. McPhaden, “Playing hide and seek with El Niño,” *Nat. Clim. Chang.* **5**, 791–795 (2015).

⁷A. Timmermann, S. I. An, J. S. Kug, F. F. Jin, W. Cai, A. Capotondi, K. Cobb, M. Lengaigne, M. J. McPhaden, M. F. Stuecker, K. Stein, A. T. Wittenberg, K. S. Yun, T. Bayr, H. C. Chen, Y. Chikamoto, B. Dewitte, D. Dommenges, P. Grothe, E. Guilyardi, Y. G. Ham, M. Hayashi, S. Ineson, D. Kang, S. Kim, W. M. Kim, J. Y. Lee, T. Li, J. J. Luo, S. McGregor, Y. Planton, S. Power, H. Rashid, H. L. Ren, A. Santoso, K. Takahashi, A. Todd, G. Wang, G. Wang, R. Xie, W. H. Yang, S. W. Yeh, J. Yoon, E. Zeller, and X. Zhang, “El Niño–Southern Oscillation complexity,” *Nature* **559**, 535–545 (2018).

⁸J. D. Neelin, D. S. Battisti, A. C. Hirst, F. F. Jin, Y. Wakata, T. Yamagata, and S. E. Zebiak, “ENSO theory,” *J. Geophys. Res. Ocean.* **103**, 14261–14290 (1998).

⁹F. F. Jin, “An equatorial ocean recharge paradigm for ENSO. Part I: conceptual model,” *J. Atmos. Sci.* **54**, 811–829 (2000).

¹⁰J. A. Knox and P. N. Knox, *Atmospheric/General circulation* (John Wiley and Sons, Ltd, 2017).

¹¹H. E. Stanley and V. K. Wong, “Introduction to phase transitions and critical phenomena,” *Phys. Today* **26**, 71–72 (1973).

¹²D. Sornette, *Crit. Phenom. Nat. Sci.* (Springer Science & Business Media, 2006) p. 395.

¹³X. Zhang, G. Hu, Y. Zhang, X. Li, and X. Chen, “Finite-size scaling of correlation functions in finite systems,” *Sci. China Physics, Mech. Astron.* **61**, 120511 (2018).

¹⁴K. Stein, A. Timmermann, and N. Schneider, “Phase synchronization of the El Niño–Southern oscillation with the annual cycle,” *Phys. Rev. Lett.* **107**, 128501 (2011).

¹⁵S. McGregor, A. Timmermann, N. Schneider, M. F. Stuecker, and M. H. England, “The effect of the south Pacific convergence zone on the termination of El Niño events and the meridional asymmetry of ENSO,” *J. Clim.* **25**, 5566–5586 (2011).

- ¹⁶M. F. Stuecker, A. Timmermann, F. F. Jin, S. McGregor, and H. L. Ren, “A combination mode of the annual cycle and the El Niño/Southern Oscillation,” *Nat. Geosci.* **6**, 540–544 (2013).
- ¹⁷H. L. Ren, J. Zuo, F.-F. Jin, and M. F. Stuecker, “ENSO and annual cycle interaction: the combination mode representation in CMIP5 models,” *Clim. Dyn.* **46**, 3753–3765 (2016).
- ¹⁸E. Guilyardi, A. Wittenberg, A. Fedorov, M. Collins, C. Z. Wang, A. Capotondi, G. J. V. Oldenborgh, and T. Stockdale, “Understanding El Niño in ocean-atmosphere general circulation models: progress and challenges,” *Bull. Am. Meteorol. Soc.* **90**, 325–340 (2009).
- ¹⁹F. F. Jin, J. D. Neelin, and M. Ghil, “El Niño on the devil’s staircase: annual subharmonic steps to chaos,” *Science* **264**, 70–72 (1994).
- ²⁰E. Tziperman, L. Stone, M. A. Cane, and H. Jarosh, “El Niño chaos: overlapping of resonances between the seasonal cycle and the Pacific ocean-atmosphere oscillator,” *Science* **264**, 72–74 (1994).
- ²¹K. Stein, A. Timmermann, N. Schneider, F.-F. Jin, and M. F. Stuecker, “ENSO seasonal synchronization theory,” *J. Clim.* **27**, 5285–5310 (2014).
- ²²M. F. Stuecker, F.-F. Jin, and A. Timmermann, “El Niño–Southern Oscillation frequency cascade,” *Proc. Natl. Acad. Sci.* **112**, 13490–13495 (2015).
- ²³A. V. Fedorov, S. L. Harper, S. G. Philander, B. Winter, and A. Wittenberg, “How predictable is El Niño?” *Bull. Am. Meteorol. Soc.* **84**, 911–919 (2010).
- ²⁴W. S. Kessler, “Is ENSO a cycle or a series of events?” *Geophys. Res. Lett.* **29**, 40–44 (2002).
- ²⁵M. E. J. Newman, “Finding community structure in networks using the eigenvectors of matrices,” *Phys. Rev. E* **74**, 1–19 (2006).
- ²⁶Y. W. Zhang, G. K. Hu, X. S. Chen, W. Chen, and W. Q. Liu, “Study of the shear-rate dependence of granular friction based on community detection,” *Sci. China Physics, Mech. Astron.* **62**, 40511 (2019).
- ²⁷T. Hofmann, “Unsupervised Learning by Probabilistic Latent Semantic Analysis,” *Mach. Learn.* **42**, 177–196 (2001).
- ²⁸A. Hannachi, I. T. Jolliffe, and D. B. Stephenson, “Empirical orthogonal functions and related techniques in atmospheric science: A review,” *Int. J. Climatol.* **27**, 1119–1152 (2007).
- ²⁹Y. Zhang, J. M. Wallace, and D. S. Battisti, “ENSO-like interdecadal variability: 1900–93,” *J. Clim.* **10**, 1004–1020 (1997).
- ³⁰R. Kawamura, “A rotated EOF analysis of global sea surface temperature variability with interannual and interdecadal scales,” *J. Phys. Oceanogr.* **24**, 707–715 (1994).
- ³¹S. McGregor, N. Ramesh, P. Spence, M. H. England, M. J. McPhaden, and A. Santoso, “Meridional movement of wind anomalies during ENSO events and their role in event termination,” *Geophys. Res. Lett.* **40**, 749–754 (2013).
- ³²J. F. Donges, Y. Zou, N. Marwan, and J. Kurths, “Complex networks in climate dynamics,” *Eur. Phys. J. Spec. Top.* **174**, 157–179 (2009).
- ³³J. F. Donges, Y. Zou, N. Marwan, and J. Kurths, “The backbone of the climate network,” *EPL* **87**, 48007 (2009).
- ³⁴K. Yamasaki, A. Gozolchiani, and S. Havlin, “Climate networks around the globe are significantly affected by El Niño,” *Phys. Rev. Lett.* **100**, 228501 (2008).
- ³⁵J. Ludescher, A. Gozolchiani, M. I. Bogachev, A. Bunde, S. Havlin, and H. J. Schellnhuber, “Very early warning of next El Niño,” *Proc. Natl. Acad. Sci.* **111**, 201323058 (2014).
- ³⁶J. Fan, J. Meng, Y. Ashkenazy, S. Havlin, and H. J. Schellnhuber, “Network analysis reveals strongly localized impacts of El Niño,” *Proc. Natl. Acad. Sci.* **114**, 7543–7548 (2017).
- ³⁷J. Meng, J. Fan, Y. Ashkenazy, and S. Havlin, “Percolation framework to describe El Niño conditions,” *Chaos An Interdiscip. J. Nonlinear Sci.* **27**, 035807 (2017).
- ³⁸Y. Zhang, J. Fan, X. Chen, Y. Ashkenazy, and S. Havlin, “Significant impact of Rossby waves on air pollution detected by network analysis,” *Geophys. Res. Lett.* **46**, 12476–12485 (2019).
- ³⁹Y. Zhang, D. Chen, J. Fan, S. Havlin, and X. Chen, “Correlation and scaling behaviors of fine particulate matter (PM_{2.5}) concentration in China,” *EPL* **122**, 58003 (2018).
- ⁴⁰J. F. Donges, I. Petrova, A. Loew, N. Marwan, and J. Kurths, “How complex climate networks complement eigen techniques for the statistical analysis of climatological data,” *Clim. Dyn.* **45**, 2407–2424 (2015).
- ⁴¹M. Wiedermann, A. Radebach, J. F. Donges, J. Kurths, and R. V. Donner, “A climate network-based index to discriminate different types of El Niño and La Niña,” *Geophys. Res. Lett.* **43**, 7176–7185 (2016).
- ⁴²X. Li and X. Chen, “Critical behaviors and finite-size scaling of principal fluctuation modes in complex systems,” *Commun. Theor. Phys.* **66**, 355 (2016).
- ⁴³G. Hu, T. Liu, M. Liu, W. Chen, and X. Chen, “Condensation of eigen microstate in statistical ensemble and phase transition,” *Sci. China Physics, Mech. Astron.* **62**, 990511 (2019).
- ⁴⁴D. P. Dee, S. M. Uppala, A. J. Simmons, P. Berrisford, P. Poli, S. Kobayashi, U. Andrae, M. A. Balmaseda, G. Balsamo, and P. Bauer, “The ERAInterim reanalysis: configuration and performance of the data assimilation system,” *Q. J. R. Meteorol. Soc.* **137**, 553–597 (2011).
- ⁴⁵A. H. Oort and J. J. Yienger, “Observed interannual variability in the Hadley circulation and its connection to ENSO,” *J. Clim.* **9**, 2751–2767 (1996).